Heliyon 10 (2024) e38153

Contents lists available at ScienceDirect

Heliyon

journal homepage: www.cell.com/heliyon

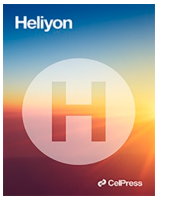

Research article

Gliomedin drives gastric cancer cell proliferation and migration, correlating with a poor prognosis

Xue You [a,*], Minghe Wang [b], Xuejing Wang [b], Xiaotong Wang [c], Yuting Cheng [c], Chuan Zhang [b], Qingrun Miao [b], Ying Feng [a,**]

[a] *Lin He's Academician Workstation of New Medicine and Clinical Translation, Jining Medical University, 133 Hehua Road, Jining, Shandong, 272067, PR China*
[b] *College of Second Clinical Medical, Jining Medical University, Jining, Shandong, 272067, PR China*
[c] *College of Basic Medicine, Jining Medical University, Jining, Shandong, 272067, PR China*

ARTICLE INFO

Keywords:
Gliomedin
Gastric cancer
Viability
Proliferation and migration
RNA-Sequencing
Poor prognosis

ABSTRACT

Gastric cancer (GC) is a prevalent global malignancy, often diagnosed at advanced stage due to a lack of early symptoms and reliable markers. Previous research has identified gliomedin (GLDN) as a potential predictive marker for poor prognosis in cancer patients. However, the specific relationship between GLDN expression and GC prognosis has been unclear. Using the Tumor-Immune System Interaction Database (TISIDB), we examined GLDN expression in GC tissues and found a positive correlation with advanced clinical stages. Kaplan-Meier Plotter analysis further demonstrated that elevated GLDN levels were closely associated with poor prognosis in GC patients. To explore the functional significance of GLDN in GC, we conducted experiments involving GLDN overexpression and knockdown in GC cell lines, as well as subcutaneous tumor formation in nude mice. Our findings provided compelling evidence that GLDN promotes GC cell proliferation, viability, and migration, significantly enhancing tumor growth in vivo. Mechanistically, RNA-sequencing (RNA-seq) combined with bioinformatics analysis revealed that GLDN influences genes enriched in the p53 signaling pathway. Our data suggest that GLDN likely regulates cell proliferation through the p53-p21-CyclinD/CDK4 signaling axis. In conclusion, our study underscores GLDN's critical role in regulating GC cell proliferation and migration, and proposes its potential as a prognostic marker for GC patients.

1. Introduction

Gastric cancer (GC) is a major global cause of cancer-related mortality, with over a million new cases and nearly 800,000 deaths reported annually [1]. This burden is particularly heavy in developing countries, with China alone accounting for more than 40 % of new cases and deaths associated with GC [2]. The lack of comprehensive screening markers and the subtlety of early symptoms result in GC being diagnosed at an advanced stages. Consequently, GC ranks as the third leading cause of cancer-related deaths worldwide, with five-year survival rates remaining limited [3,4]. Currently, the primary treatments for GC include surgery, chemotherapy, and/or radiotherapy. To improve outcomes, it is crucial to unravel the molecular mechanisms underlying GC initiation and progression. This

* Corresponding author.
** Corresponding author.
E-mail addresses: youxue19910@mail.jnmc.edu.cn (X. You), fengying@sinh.ac.cn (Y. Feng).

https://doi.org/10.1016/j.heliyon.2024.e38153
Received 30 May 2024; Received in revised form 18 September 2024; Accepted 18 September 2024
Available online 19 September 2024

understanding can lead to the identification of potential targets for early diagnosis and treatment, ultimately enhancing survival rates and patient care.

Gliomedin (GLDN), also known as CRG-L2 (cancer related gene-liver 2), is a type-II membrane protein containing 551 amino acids. GLDN plays significant roles in both physiological and pathological contexts. Mutations in GLDN are associated with several disorders, including impaired heel bone strength and the development of fatal congenital polyarticular contracture syndrome [5,6]. Beyond its involvement in these conditions, GLDN is a key player in cell motility and cellulose degradation, serving as the core component of the type IX secretion system [7].

Previous studies have intriguingly highlighted GLDN as a significant marker for both predicting and assessing prognosis in various human cancers. Intitially, GLDN was identified as highly expressed in human hepatocellular carcinoma (HCC) while showing limited expressions in normal human tissues [8]. Its distinctive upregulation in early tumor development positioned GLDN as a potential marker. Further research confirmed its strong association with the prognosis of HCC patients [9]. In addition, GLDN exhibits tumor-suppressive properties in colorectal cancer (CRC), where it has been suggested as a potential prognostic predictor for CRC patients [10]. In melanoma, GLDN has emerged as a novel predictive biomarker, and in lung adenocarcinoma, it is linked to acquired resistance to epidermal growth factor receptor-tyrosine kinase inhibitors (EGFR-TKIs) [11,12]. Despite these findings, it remains unclear whether GLDN expression is elevated in GC and whether it correlates with poor prognosis in GC patients.

In this study, we utilized the Tumor-Immune System Interaction Database (TISIDB) software to analyze GLDN expression in GC tissues across various stages and grades. Our analysis revealed a positive correlation between elevated GLDN levels and advanced clinical stages of GC. Further investigation using Kaplan–Meier Plotter analysis demonstrated that increased GLDN expression is closely associated with poor prognosis in GC patients. To explore the functional role of GLDN, we conducted overexpression and knockdown experiments in GC cell lines. These experiments elucidated that GLDN promoted the proliferation and migration of GC cells. Notably, GLDN overexpression significantly enhanced tumor growth in nude mice, underscoring its critical role in GC progression. To delve deeper into the molecular mechanisms, we performed RNA-seq coupled with bioinformatic analysis. This approach revealed that genes regulated by GLDN were enriched in the p53 signaling pathway. Further evidence suggested that GLDN likely operates through the p53-p21-CyclinD/CDK4 signaling pathway to regulate cell proliferation.

2. Materials and methods

2.1. Bioinformatics analysis of GLDN expression in GC tissues and its clinical significance

TISIDB database [13] was utilized to assess the relationship between GLDN expression and the clinicopathological stages (stages 1, 2, 3 and 4) as well as tumor grades (grades 1, 2 and 3) in GC. The Spearman correlation test was used to determine the correlation coefficient (rho) and the P value, with a P value of less than 0.05 considered statistically significant [14].

The Kaplan–Meier (KM) Plotter database, accessible at https://www.kmplot.com, is employed for prognosis analysis. Based on median expression value of GLDN, GC patients were divided into high-expression and low-expression groups. A KM plot was then used to evaluate the risk prognosis, and the log-rank test was performed to compare the survival curves. Hazard ratios (HR) with 95 % confidence intervals and log-rank P-values were calculated, with P-values less than 0.05 considered statistically significant (HR greater than 1). Additionally, overall survival (OS), first progressive survival (FP) and post-progression survival (PPS) of GC patients were visualized using an updated version of the KM Plotter website [15].

2.2. Cell culture and transfection

Human GC cell line MKN28 was purchased from the BeNa Culture Collection (Beijing, China) and cultured in RPMI-1640 medium containing 10 % fetal bovine serum (FBS) and 1 % penicillin/streptomycin. Human gastric adenocarcinoma hyperdiploid (AGS) cells were purchased from the Cell Bank of Chinese Academy of Medical Science (Shanghai, China) and grown in F12K complete medium supplemented with 10 % FBS and 1 % penicillin-streptomycin. The siRNA oligos against the GLDN gene were synthesized by Gene Pharma (Suzhou, Jiangsu, China). Knockdown of GLDN was achieved by siRNA transfection of MKN28 cells using Lipofectamine™ RNAiMAX system (Thermo Fisher scientific, OH, USA) following the manufacturer's protocol.

2.3. Lentivirus production and infection

GLDN cDNA was cloned into pLVX-AcGFP-N1 vector, and stable overexpression of GLDN in AGS cell line was achieved by lentiviral infection followed by puromycin selection. Briefly, lentiviruses were generated by transient transfection with the core plasmid and viral packaging vectors (psPAX2 and pMD2G) into immortalized human embryonic kidney (HEK293) cells. The lentiviral supernatant was harvested and sterile-filtered after 48 h and 72 h separately. At 72 h after infection, stable cell lines were established by puromycin selection.

2.4. Quantitative real-time PCR (qRT-PCR)

Total RNA was extracted by TRIzol reagent (Invitrogen, CA, USA). RNA(1 μg) was reverse transcribed to cDNA with PrimerScriptTM RT reagent Kit with gDNA Eraser (TaKaRa, Dalian, China) according to the manufacturer's instructions, respectively. To detect the mRNA levels of different genes, TB™ green (TaKaRa, Dalian, China) was used for qRT-PCR performed on an ABI Prism™

7900 sequence detection system according to the manufacturer's protocol; the specific primers used are shown in Table S1.

2.5. Cell viability and proliferation assays

For the CCK8 assay, siRNA-transfected MKN28 cells were seeded in 96-well plates at a density of 5000 cells/well with fresh medium, AGS stable cells were seeded 2000 cells/well. After incubation at 37 °C with 5%CO2, 10 μl of CCK8 (HanBio, Shanghai, China) reagent was added to each well and cultured for another 2 h. Cell viability was calculated by measuring the absorbance at 450 nm. For the colony formation survival assay, cells were plated in 6-well plates at 1000 cells/well for AGS cells. After two weeks, the colonies were photographed and counted after paraformaldehyde fixation and crystal violet staining. Four regions were randomly selected as the statistics of the number of colonies in the corresponding group. For the EdU incorporation assay, cells were cultured in 96-well plates, and cell replication ability was detected using the Cell-Light EdU Apollo488 In Vitro Kit (Ribobio, Guangzhou, China).

2.6. Cell migration assays

For the transwell assay, cells (AGS for 3×10^4, and MKN28 for 1×10^5) were suspended and seeded into the upper chambers of the transwell plates in serum-free medium, and10 % FBS was added to the lower chamber. After 48 h, the cells in the upper chamber were removed, and the migrated cells on the bottom surface were fixed with paraformaldehyde and stained with crystal violet. For the wound-healing assay, cells were cultured in 6-well plate overnight. Three scratches were made per well using a 200 μl pipette tip across the center and sides of the culture plate. After washing three times with PBS, the cells were cultured in serum-free medium and imaged under a microscope at 24 h.

2.7. Western blotting analysis

Cultured cells were collected from RIPA lysis buffer with protease inhibitors (Beyotime, Jiangsu, China). The extracted protein was electrophoresed by 10 % and 12 % SDS-PAGE gels and transferred to an activated PVDF membrane for 1 h. After being blocked in 3 % bovine serum albumin (BSA) for 90 min, the primary antibodies diluted in the block solution were incubated at 4 °C overnight, and HRP-coupled secondary antibodies were incubated at room temperature for 90 min. Finally, the protein bands were quantified by an enhanced chemiluminescence (ECL) luminescent substrate (Millipore, MA, USA). The antibodies used in the study were as follows: anti-p53 (Proteintech, IL, USA), anti-p21 (Proteintech, IL, USA), anti-CyclinD1 (ABclonal, MA, USA), anti-CyclinD3 (ABclonal, MA, USA), anti-CDK4 (ABclonal, MA, USA), anti-GLDN (Biorbyt, UK), anti-Actin (Affinity, OH, USA), and anti-GAPDH (Proteintech, IL, USA).

2.8. Subcutaneous tumor formation experiment in nude mice

Control and GLDN-OV AGS cells were harvested and utilized in subcutaneous tumor formation experiments. These cells underwent two washes with PBS and two additional washes with serum-free F12K medium. They were then injected into the hindlimb area to stiumlate tumor development. Tumor size was measured every other day, and the volume was calculated using the formula: $0.5 \times \text{length} \times \text{width}^2$. After the completion of the experiments, the mice were euthanized, and tumor weights were recorded.

2.9. Immunohistochemical staining of tumor tissue from nude mice

After the subcutaneous tumor tissue was removed from the mice, half of the tissue was placed in RIPA lysis buffer containing protease inhibitors, then lysed using a tissue grinder, and subseuqently used for WB analysis. The other half of the tumor tissue was fixed in 4 % paraformaldehyde overnight, dehydrated with graded ethanol, cleared with xylene, immersed in wax, and embedded. The wax block was then positioned on a paraffin microtome and sectioned. These sections were dewaxed with xylene and rehydrated with gradient ethanol. Antigen retrieval was performed in 0.01M sodium citrate buffer, and endogenous peroxidase activity was quenched with 0.3 % H_2O_2/methanol solution. The section were blocked in 5 % sheep serum for 1 h at room temperature, followed by overnight incubation with the primary antibody at 4 °C and then secondary antibody at room temperature for 1 h. After staining the sections with DAB chromogenic solution, the nuclei were counterstained with DAPI, and the sections were sealed and photographed under a microscope.

2.10. RNA-seq library generation and analysis

Total RNAs were extracted from stable AGS/GLDN-OV and control cells, which were used for cDNA library construction and paired-end reads sequencing. Analysis and data mining were performed using the Dr. Tom Multi-omics Data mining system, as described previously [16]. Briefly, after the raw data obtained by RNA-sequencing was subjected to quality control, the clean reads obtained by filtering with SOAPnuke were aligned to the reference genome sequence using HISAT, and Bowtie2 was used to compare the clean reads with the reference genes. Finally, quantitative and differential gene expression analyses were performed after the second quality control step [17]. Three replicates were prepared, sequenced, and analyzed separately.

2.11. Analysis of differentially expressed genes (DEGs)

Volcano plots and heat maps generated by Dr. Tom's software were used to display the differential gene expression between the control group and the GLDN-OV group (n = 3). The DEGs were identified according to the criteria of $|\log2FC| \geq 0.5$, Qvalue ≤ 0.05.

2.12. Gene ontology (GO), Kyoto encyclopedia of genes and genomes (KEGG) and gene set enrichment analysis (GSEA)

GO and KEGG enrichment analyses were conducted using the Dr. Tom web-based solution [18]. Briefly, to further explore the gene functions related to the changes in differential genes, GO and KEGG enrichment analysis of differential genes was performed using the Phyper function in R software based on the hypergeometric test. The P value was calculated and corrected by false discovery rate (FDR) to obtain the definition of a satisfying $Q_{value} \leq 0.05$, which was clarified as significant enrichment in candidate genes. For GSEA, the GENE DENOVO website (https://www.omicshare.com/tools/Home/Soft/gsea) was used to analyze gene expression data from Control and GLDN-OV groups. ES values were calculated for each gene set, revealing biological processes or pathways associated with GLDN overexpression. Blue to red indicates increased expression, with positive ES value (red) indicating upregulation and negative ES value (green) indicating downregulation.

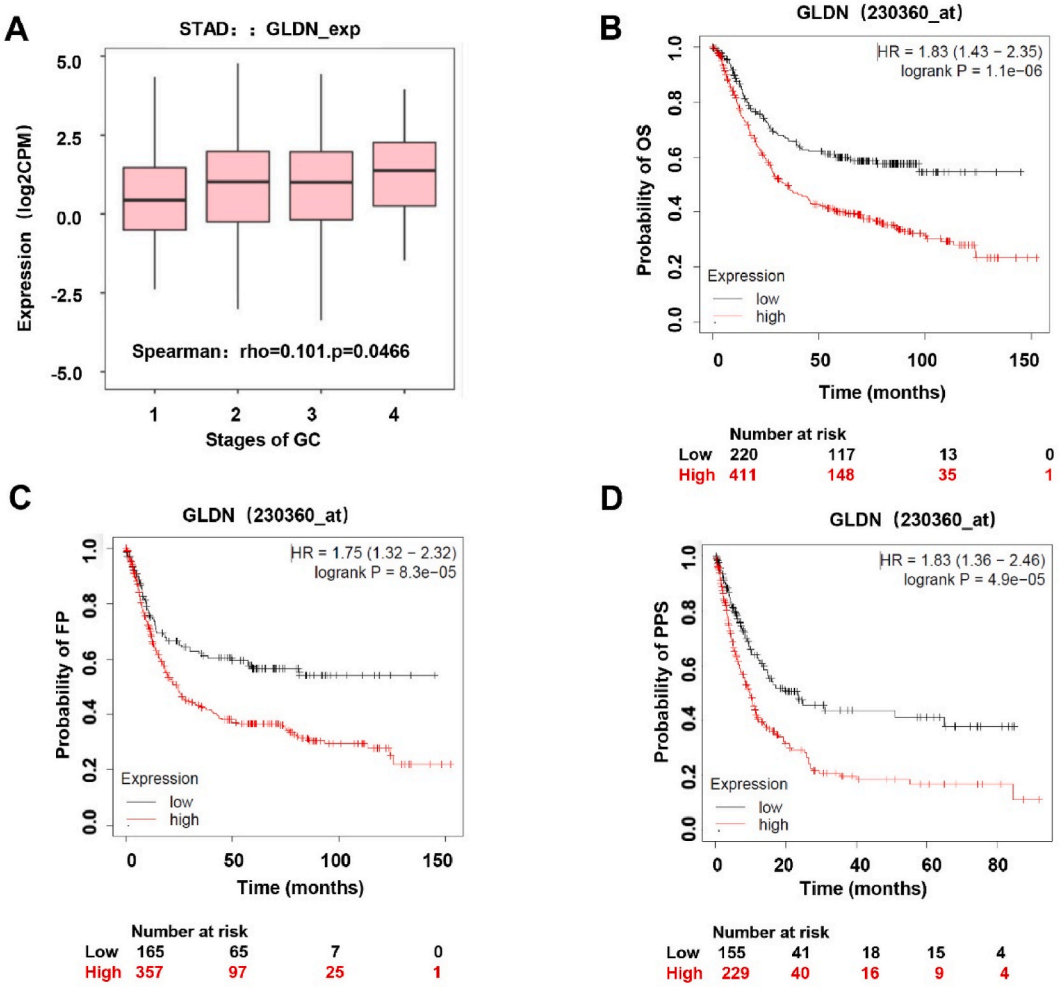

Fig. 1. Bioinformatics analysis of GLDN expression in GC tissues and its clinical significance. (A) GLDN expression levels in GC tissues were analyzed across different stages using the TISIDB software. The p-value was obtained by comparing GLDN expression across the four cancer stages (1, 2, 3, and 4) of stomach adenocarcinoma (STAD). **(B–D)** Kaplan-Meier curves illustrates the correlation between GLDN expression and the prognosis of GC patients in terms of overall survival (OS) (B), first progression survial (FP) (C), and post-progression survival (PPS) (D). HR (hazard ratio) = 1.83(1.43–2.35), logrank P = 1.1e-06 for OS (Fig. 1B); HR = 1.75(1.32–2.32), logrank P = 8.3e-05 for FP (Fig. 1C); HR = 1.83(1.36–2.46), logrank P = 4.9e-05 for PPS (Fig. 1D). *** indicates a P-value <0.001 calculated using the log-rank test.

2.13. Statistical analysis

The analysis of RNA-seq data involved several steps. Firstly, RSEM was employed to calculate the gene expression level for each sample. The identification of Differentially expressed genes (DEGs) was carried out using the DESeq2 method, which is based on the negative binomial distribution principle. Subsequently, the R package pheatmap was utilized for hierarchical cluster analysis, incorporating moderated estimation of fold change and dispersion for RNA-seq data with DESeq2. The normal distribution of experimental data was assessed using the Shapiro-Wilk normality test in GraphPad Prism software. All experimental data are presented as the mean ± standard deviation (SD). Statistical comparisons between two groups were performed using an unpaired two-tailed Student's t-test. For each KM plot, the log-rank test was employed for statistical analysis. Quantitative statistics of protein bands was conducted by assessing relative intensity with ImageJ software. Each experiment was independently repeated at least three times. Statistical significance levels were denoted as follows: * for $p < 0.05$ (statistically significant), ** for $p < 0.01$ (highly significant), and *** for $p < 0.001$ (extremely significant).

3. Results

3.1. The expression of GLDN correlates with the prognosis of GC patients

To investigate the potential significance of GLDN in GC, we utilized the TISIDB software to analyze GLDN expression in GC tissues at various stages and grades. Our results showed a positive correlation between GLDN expression and the clinical stages of GC (Fig. 1A). However, no significant correlation was observed between GLDN expression and different tumor grades (Supplemental Fig. 1). To further understand the impact of GLDN expression on GC patients, we employed the Kaplan–Meier Plotter online database to generate survial curves. The analysis revealed that higher GLDN expression was significantly associated with poorer overall survival (OS), first progression survial (FP), and post-progression survival (PPS) in GC patients (Fig. 1B–D). These findings suggest that GLDN expression is linked to the prognosis of GC patients.

3.2. GLDN was highly expressed in MKN28 cells but exhibited low expression levels in AGS cells

Next, we examined GLDN protein expression in two gastric cancer cell lines: AGS and MKN28. Western blotting (WB) analysis showed that GLDN expression was significantly higher in MKN28 cells compared to AGS cells, where it was expressed at much lower levels (Fig. 2A). To investigate whether GLDN overexpression influences cell proliferation, we created stable cell pools overexpressing GLDN in AGS (AGS/GLDN-OV) using a lentiviral infection system. We also generated control cell lines (AGS/Con) expressing empty vectors. WB analysis confirmed that GLDN protein levels were significantly increased in AGS/GLDN-OV cells compared to controls (Fig. 2B).

3.3. GLDN overexpression enhances the viability, proliferation and migration of AGS cells

We conducted CCK-8 assays to evaluate the effect of GLDN overexpression on cancer cell proliferation. As shown in Fig. 3A, elevated GLDN levels significantly promoted the proliferation of AGS cells. The colony formation assay further demonstrated that GLDN overexpression markedly increased the survival capacities of AGS cells compared to control cells (Fig. 3B). To further evaluate cell proliferation, we employed the thymide analog, EdU, which incorporates into cellular DNA during DNA replication. The results showed a higher number of EdU + cells in AGS/GLDN-OV cells compared to control cells (Fig. 3C).

Beyond proliferation, we examined the impact of GLDN on cancer cell migration. Transwell assays (Fig. 3D) and scratch wound

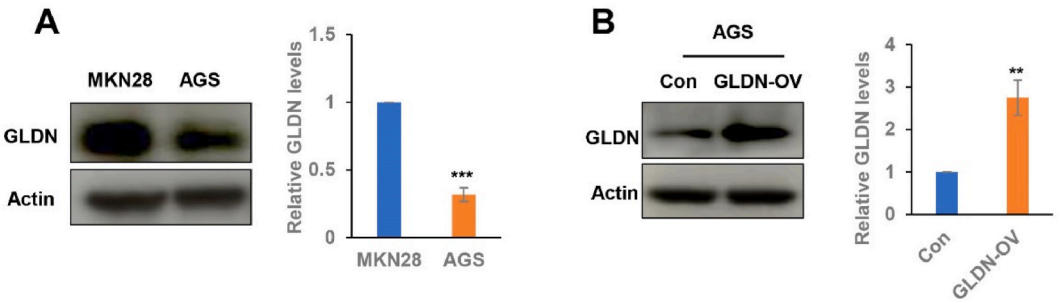

Fig. 2. GLDN was highly expressed in MKN28 cells but exhibited low expression levels in AGS cells. **(A)** GLDN protein levels in two GC cell lines (MKN28 and AGS) were assessed by WB. Quantification of GLDN protein levels in these cells is shown on the right. **(B)** AGS cells were infected with lentivirus carring GLDN and a control vector, respectively, followed by puromycin screening. WB analysis was performed to confirm GLDN expression in stable AGS/GLDN-OV cells. Quantification of GLDN protein levels is displayed on the right. All the data are shown as mean ± SD, with **, and *** indicating significant levels of $P < 0.01$, and $P < 0.001$, respectively, between groups. Non-adjusted images of blots are shown in Supplementary Fig. 2.

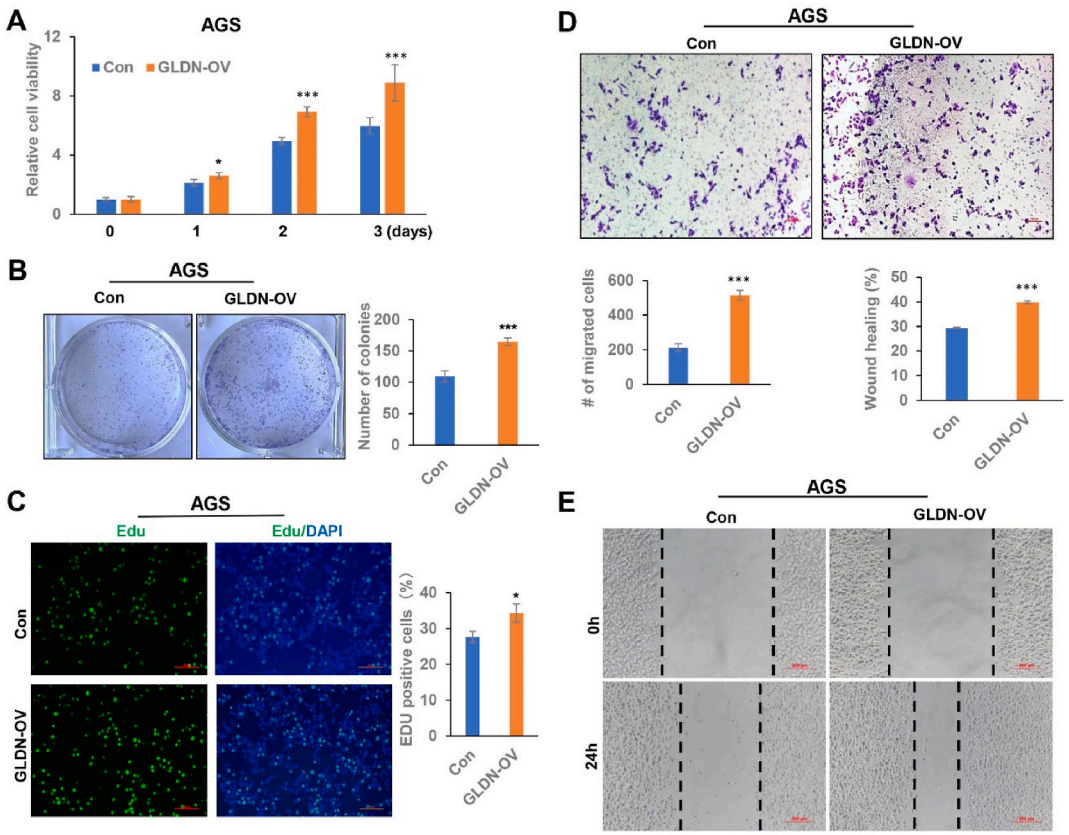

Fig. 3. GLDN overexpression enhances the viability, proliferation and migration of AGS cells. (A) CCK-8 assays were performed to detect the effect of GLDN overexpression on cancer cell proliferation, using AGS/GLDN-OV and control cells. **(B)** Clonogenic survival assays were performed using AGS/GLDN-OV and control cells. Representative images of cells stained with crystal violet are shown, and the quantified number of colonies is presented on the right. **(C)** Images of EdU staining (scales bar, 200 μm) are displayed, and a comparison of EdU-positive rates among the indicated cells is provided on the right. (**D**) Transwell cell migration assays were performed with AGS/GLDN-OV cells. Representative images of cells stained with crystal violet were shown and quantification was displayed at the bottom left of the images (scales bar, 100 μm). **(E)** Scratch-wound assays were performed with AGS/GLDN-OV and control cells. Representative microscope images of cells were shown and quantification is presented at the top right of the images (scales bar, 200 μm). All the data are presented as mean ± SD, ** indicates $P < 0.01$, and ***$P < 0.001$. (For interpretation of the references to color in this figure legend, the reader is referred to the Web version of this article.)

assays (Fig. 3E) were performed with AGS/GLDN-OV and control cells. The findings indicated that GLDN overexpression significantly enhanced the migratory capabilities of AGS cells compared to the control cells. Collectively, these results suggest that GLDN plays a pivotal role in enhancing both cancer cell proliferation and migration.

3.4. GLDN knockdown inhibits GC cell proliferation and migration

Next, we investigated the effects of GLDN knockdown in GC cells. To achieve this, we designed siRNAs specifically targeting GLDN (siGLDN) and used control siRNAs (siCon) for comparison. Notably, our initial analysis showed high GLDN expression in MKN28 cells (Fig. 2A). Therefore, we focused on evaluating the effects of siRNA-mediated GLDN knockdown in these cells.

As shown in Fig. 4A and B, treatment with siGLDN significantly reduced both mRNA and protein levels of GLDN within MKN28 cells compared to siCON treatment. In contrast to the results observed with GLDN overexpression, GLDN knockdown in MKN28 cells led to a marked inhibition on cancer cell proliferation and migration. These effects were quantitatively assessed through CCK-8 and transwell assays (Fig. 4C and D). In summary, our findings underscore the pro-tumorigenic role of GLDN in gastric cancer cells.

3.5. RNA-seq analysis and enrichment analysis of DEGs

To explore the underlying mechanisms responsible for the pro-tumorigenic effects of GLDN in GC cells, we performed RNA-seq analysis using total RNA extracted from AGS/GLDN-OV and control cells. Our analysis unveiled a total of 428 DEGs affected by GLDN overexpression compared to the control group. These DEGs are strikingly illustrated in the volcano plot, with 233 genes (54.44 %) up-regulated and 195 genes (45.56 %) down-regulated in GLDN-OV cells (Fig. 5A). Furthermore, we generated a heatmap

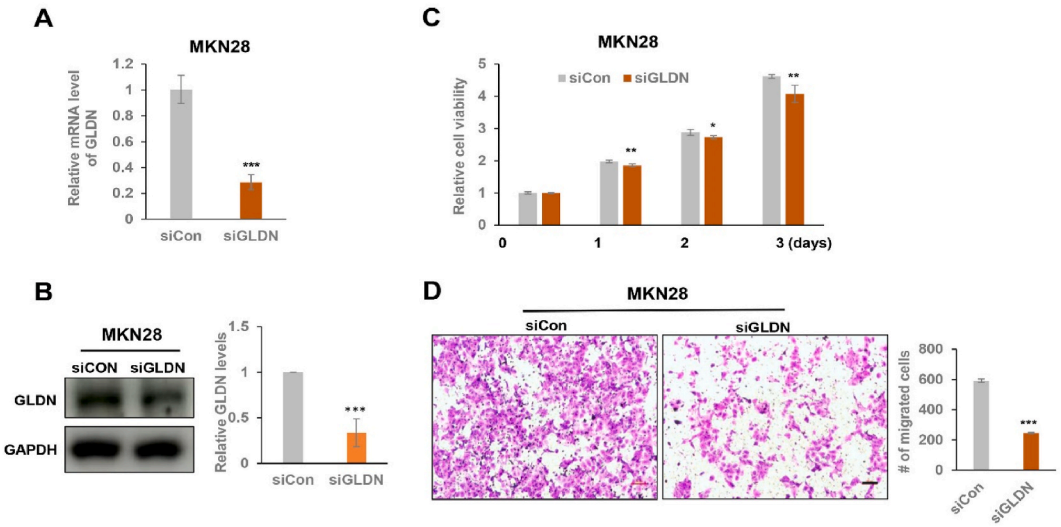

Fig. 4. GLDN Knockdown reduces viability and migration of MKN28 cells. (A) qRT-PCR analysis was performed using total RNA extracted from MKN28 cells that were transiently transfected with control or GLDN-specific siRNA. **(B)** The knockdown efficiency was assessed by WB and the quantification of GLDN levels is displayed on the right. **(C)** CCK-8 assays were performed with MKN28 cells after treatment with indicated siRNAs. **(D)** Transwell cell migration assays were performed with cells described in (A). Representative images of cells stained with crystal violet and quantification are shown (scales bar, 100 μm). All the data are shown as mean ± SD, with *, **, and *** indicating significance levels of $P < 0.05$, $P < 0.01$, and $P < 0.001$, respectively, between groups. Non-adjusted images of blots are shown in Supplementary Fig. 3. (For interpretation of the references to color in this figure legend, the reader is referred to the Web version of this article.)

displaying the expression patterns of these DEGs across three independent replicates of both experimental and control groups. In this heatmap, upregulated genes are highlighted in red, and downregulated genes are shown in blue (Fig. 5B).

To gain deeper insights into the biological functions of these DEGs, we conducted KEGG, GO, and GSEA enrichment analysis. The KEGG analysis identified enriched pathways related to cell migration, such as tight junction, regulation of actin cytoskeleton and focal adhesion. Additionally, other enriched pathways, including cellular senescence, prostate cancer, and the PI3K-Akt signaling pathway were all associated with cell proliferation (Fig. 5C). The GO analysis of Biological Processes (BP) revealed significant enrichement in processes like ribosome biogenesis, and actomyosin structure organization, among others (Fig. 5D). Furthermore, the GSEA analysis demonstrated that these DEGs were significantly enriched in pathways associated with breast cancer relapse, targets of CCND1 and CDK4, and p53-related processes (Fig. 5E). These enrichement analyses are fully consistent with the in vitro function of GLDN, which promotes both cell migration and cell proliferation.

3.6. *GLDN negatively regulates the p53-mediated signaling pathway*

GSEA analysis revealed a subset of genes signficiantly affected by GLDN overexpression, and intricately involved in the p53 signaling pathway (Fig. 6A). To validate these findings, we selected 10 genes for qRT-PCR analysis. As shown in Fig. 6B, genes related to cell cycle regulation, such as *CCND1* (cyclin D1), *CCND3* (cyclin D3), *CCNE1* (cyclin E1), and *CDK6* (cyclin dependent kinase 6), showed marked increases in expression. In contrast, molecules involved in inhibiting cell growth or promoting apoptosis exhibited opposite trends. DYRK2, a pro-apoptotic kinase [19], was significantly down-regulated, along with MYBBP1A and STEAP3, both known tumor suppressors [20]. DKK1, a key antagonist of the Wnt/β-catenin signaling pathway [21], was also significantly decreased. Conversely, RRM2 (ribonucleotide reductase regulatory subunit M2), crucial for DNA metabolism [22], and *THBS1* (thrombospondin 1), which inhibits tumor cell invasion and growth [23], both showed significant increases. Our qRT-PCR validation closely matched the RNA-seq analysis, confirming the reliability of these findings (Fig. 6C).

We further conducted WB analysis to examine the protein-level effects of GLDN on genes involved in the p53 signaling pathway. In MKN28 cells, GLDN knockdown led to increased levels of p53 and its downstream effector, p21 (Fig. 6D). p21 is known to form complexes with cyclinD/CDK4 to induce cell cycle arrest in the G1 phase [24]. Consequently, decreased levels of CCND1, CCND3 and CDK4 were observed after GLDN knockdown compared to the control (Fig. 6D). Conversely, GLDN overexpression produced opposite effects: reduced p21 and p53 protein levels, and increased CCND1, CCND3 and CDK4 levels in AGS cells (Fig. 6E). These findings suggest that GLDN affects prolfieraiton of GC cells predominantly through the regulation of the p53-mediated signaling pathway.

3.7. *GLDN promotes gastric cancer growth in nude mice*

To investigate the potential of GLDN to promote the growth of GC cells in vivo, we conducted subcutaneous tumor formation experiments in nude mice. Subsequently, we separately injected stable AGS/GLDN-OV and control cells subcutaneously into nude

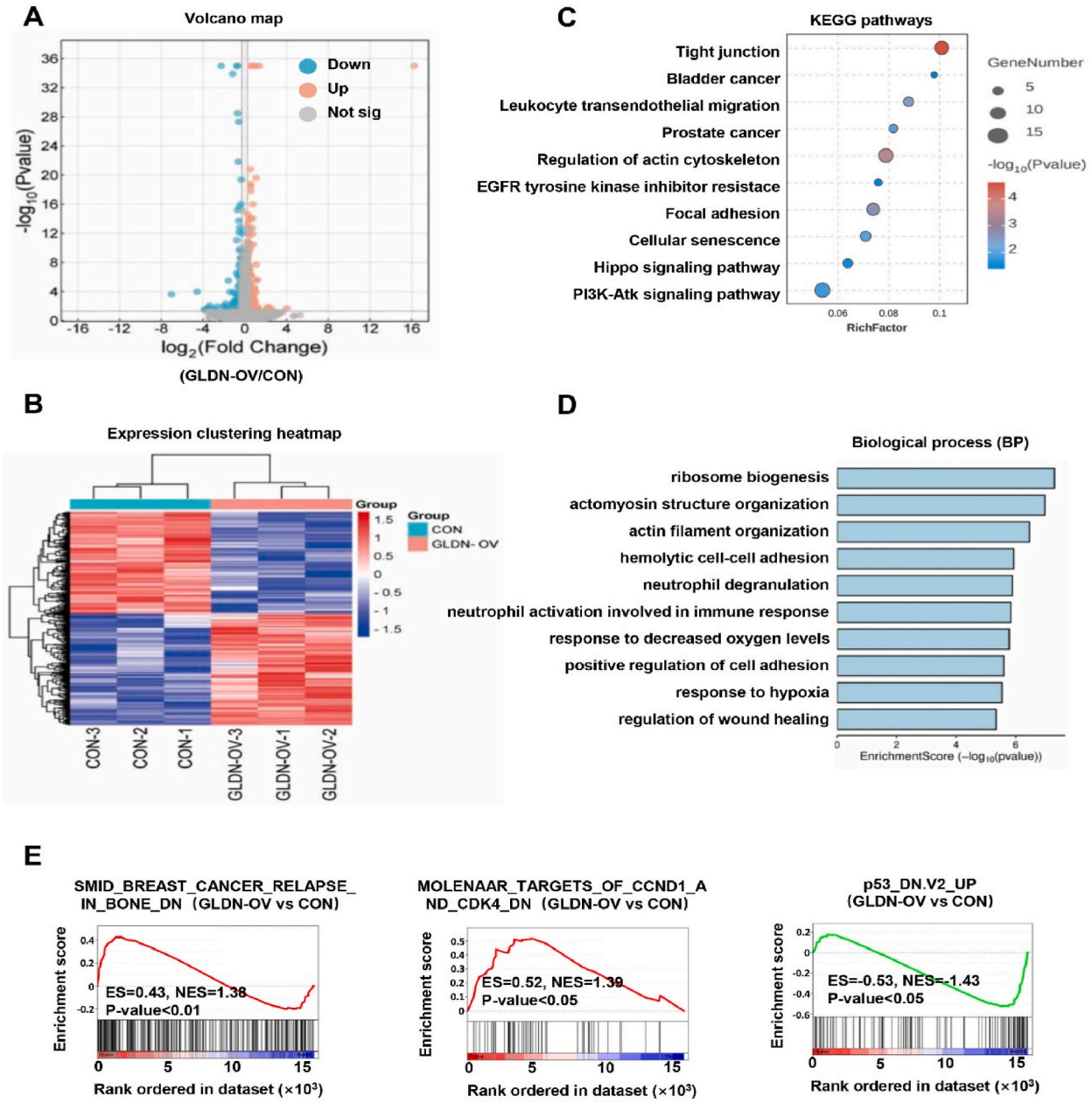

Fig. 5. RNA-seq analysis and enrichment analysis of DEGs. (A) Volcano plot illustrating DEGs between the GLDN-OV and control cells. **(B)** Heatmap comparing DEGs across three GLDN-OV groups and three control groups. **(C)** KEGG analysis highlighting affected pathways by GLDN overexpression. **(D)** GO analysis of DEGs in the Biological Processes domain. **(E)** GSEA analysis showing pathways impacted by GLDN overexpression (red curves: upregulated, and green curves: downregulated). (For interpretation of the references to color in this figure legend, the reader is referred to the Web version of this article.)

mice. As shown in Fig. 7A, AGS cells overexpressing GLDN consistently resulted in tumors with significantly larger volumes throughout their development in nude mcie, in contrast to the control cells. Moreover, two weeks after the injection, tumors originating from AGS/GLDN-OV cells exhibited both increased size and weight in comparision to those derived from control cells (Fig. 7B and C).

To further elucidate the regulatory role of GLDN, WB analysis of tumor tissues confirmed that GLDN modulates the p53-mediated signaling pathway, consistent with cellular level findings. Specifically, tumors derived from AGS/GLDN-OV cells exhibited decreased levels of p21 and p53 proteins and increased levels of CCND1, CCND3 and CDK4 proteins compared to the control group (Fig. 7D). Additionally, we sought to validate the influence of GLDN on proliferation in vivo. Immunohistochemical staining for Ki67 in tumor tissues revealed a significant increase in Ki67-positive cells in the GLDN-overexpressing tumors relative to the controls (Fig. 7E). These findings clearly demonstrate that GLDN promotes tumorigenesis in vivo.

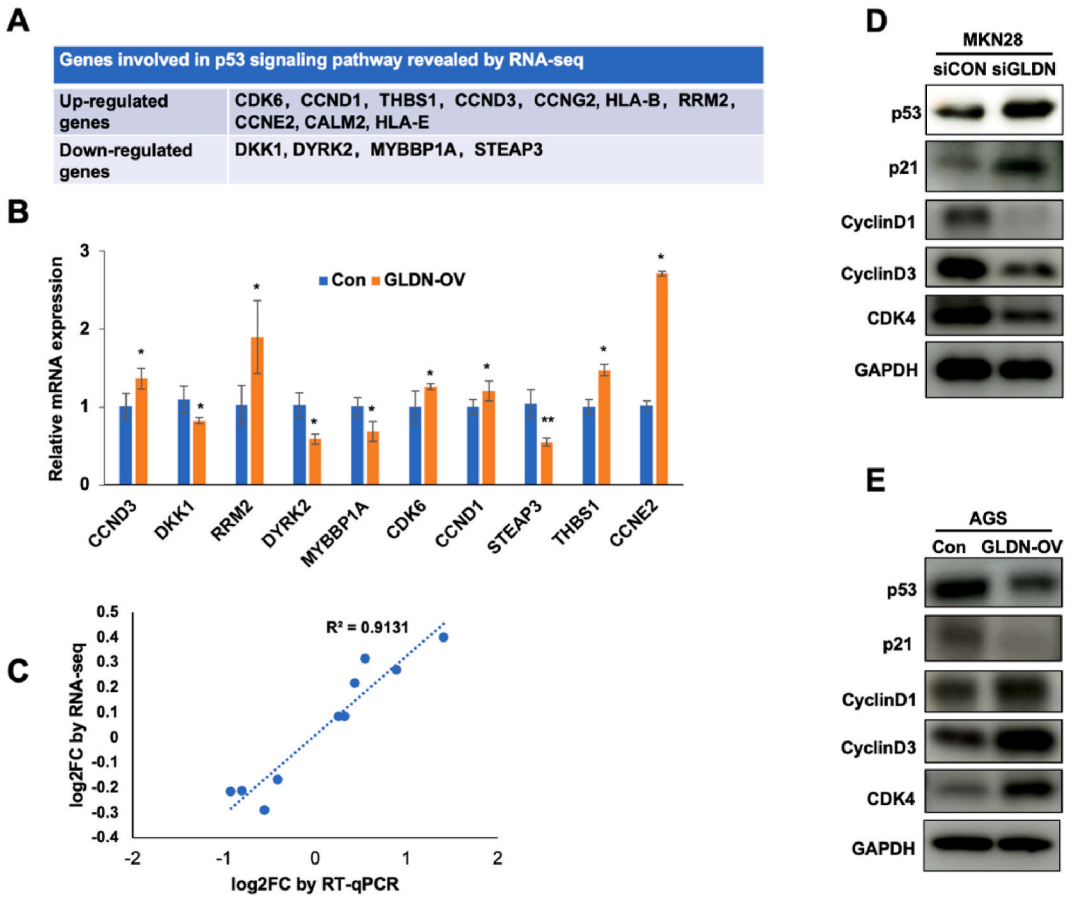

Fig. 6. GLDN regulates p53-p21-cyclinD/CDK4 signaling pathway. (A) Gene lists enriched in the p53 signaling pathway, as identified through RNA-seq analysis. **(B)** Total RNA was extracted from GLDN-overexpressing AGS cells and control cells, and expression levels of indicated genes were detected using qRT-PCR. **(C)** Scatter plots demonstrating the consistency between RNA-seq analysis and qRT-PCR results. **(D)** WB analysis was performed with indicated antibodies using whole cell lysates of MKN28 cells following siRNA treatment. **(E)** WB analysis was conducted with indicated antibodies using whole cell lysates of GLDN-overexpressing AGS cells, as well as control cells. All the data are presented as mean ± SD, * for $P < 0.05$, with ** indicating $P < 0.01$, and *** indicating $P < 0.001$ between groups. Non-adjusted images of blots are shown in Supplementary Fig. 4.

4. Discussion

Due to the high morbidity and mortality rates of GC, there is a critical need to identify early screening tumor biomarkers and understand the mechanisms underlying GC progression. Our study highlights a significant link between elevated GLDN expression and poor prognosis in GC patients. Furthermore, we demonstrate that GLDN overexpression promotes the proliferation and migration of GC cells, while GLDN knockdown inhibits these processes.

GLDN is significantly overexpressed in human HCC tissues, and its evelated levels are closely associated with an unfavorable prognosis in liver cancer patients [8,9]. Similarly, our data reveal a strong correlation between high GLDN expression and poor prognosis in GC patients. These findings strongly suggest that GLDN could serve as a valuable biomarker for assessing the prognosis of both HCC and GC patients. Interestingly, in contrast to its role in HCC and GC, high GLDN expression predicts a favorable prognosis in NSCLC (Non-small cell lung cancer) patients who have resistance to EGFR-TKI therapy [12]. Moreover, another study reported that GLDN functions as a tumor suppressor and its expression is reduced in bladder cancer [25]. These contrasting roles of GLDN in different cancer types may reflect the high heterogeneity of tumors and the complex, context-specific mechanisms involved in tumor development and progression.

The p53 signaling pathway is a crucial cellular mechanism that responds to both intracellular and extracellular stress signals to maintain cellular homeostasis [26]. As the central component of this pathway, p53 regulates key processes such as the cell cycle, DNA damage, cell differentiation, apoptosis and aging. These roles collectively underscore p53's function as a tumor suppressor gene. Our RNA-seq analysis indicates that GLDN may promote tumorigenesis in GC cells through modulation of the p53-mediated signaling pathway. Supporting this, we found that GLDN knockdown in MKN28 cells led to significant increases in the protein levels of p53 and p21, along with decreases in CyclinD1, CyclinD3 and CDK4. The activity of p53 is tightly regulated by negative feedback mechanisms

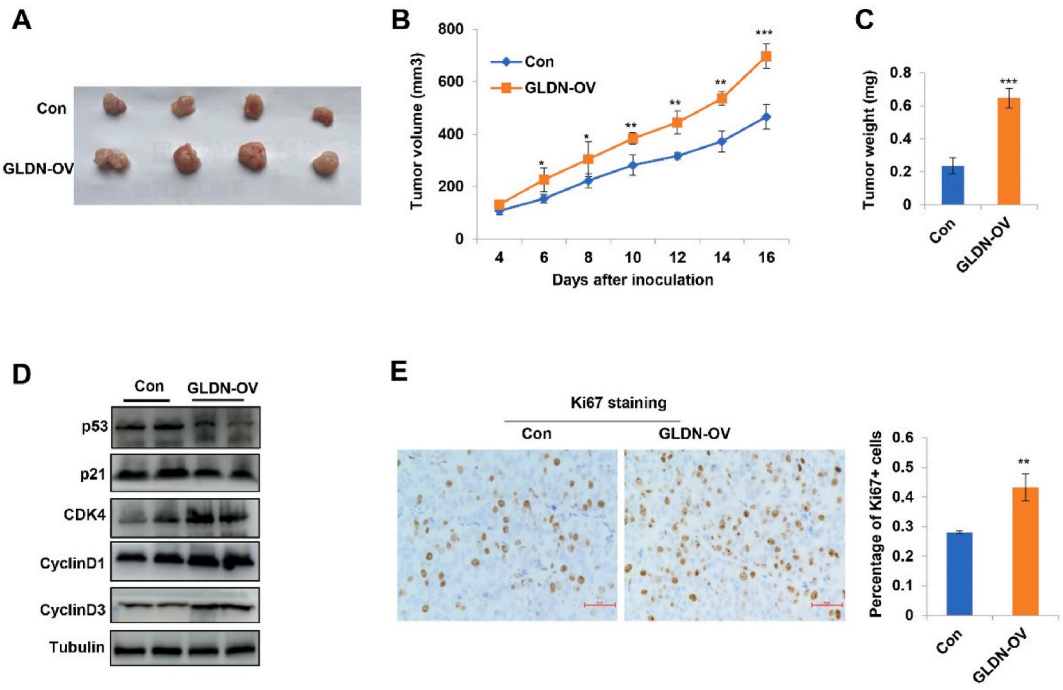

Fig. 7. GLDN promotes gastric cancer growth in vivo. **(A)** Volume measurements of tumors from mice injected subcutaneously with AGS/GLDN-OV and control group cells, respectively. **(B)** Images of tumors isolated from AGS/GLDN-OV injected mice and control mice. **(C)** A comparison of tumor weights between AGS/GLDN-OV injected mice and control mice. **(D)** WB analysis was conducted using protein extracts from tumor tissues of AGS/GLDN-OV injected mice and control mice. **(E)** Immunohistochemical staining of Ki67 in mouse tumor tissues (scales bar, 50 μm). Qualification of Ki67 signals is presented on the right graph. All the data are shown as mean ± SD, *indicates $P < 0.05$, ** indicates $P < 0.01$, and ***$P < 0.001$ between groups. Non-adjusted images of blots are shown in Supplementary Fig. 5.

involving proteins such as MDM2 (MDM2 proto-oncogene), COP1 (COP1 E3 uniquitin ligase). Among these, MDM2 is particularly crucial, as it binds to p53 and facilitates its ubiquitination and subsequent degradation, maintaining a dynamic balance of p53 protein levels [26]. Additionally, p14ARF can interact with MDM2 to enhance p53 expression by inhibiting MDM2's activity [27]. Given this, further investigation is required to determine whether GLDN directly affects p53 degradation or if it modulates the p53 signaling pathway through the MDM2-mediated degradation pathway. Understanding this will clarify the exact mechanisms by which GLDN influences the p53 signaling pathway and its role in tumorigenesis.

Our findings show that the mRNA level of DYRK2, a pro-apoptotic factor, is significantly decreased with GLDN overexpression. Additionally, DKK1, which also plays a role in inducing apoptosis and inhibiting cell proliferation [28], was observed to decrease. These results suggest that GLDN overexpression may enhance cancer cell proliferation primarily by inhibiting apoptosis in GC cells. Previous studies have demonstrated that p53 can induce cell death via the p53/Bax/caspase-3-dependent pathway [29] and regulate PUMA (p53 upregulated modulator of apoptosis) -mediated apoptosis signaling pathway [30]. Furthermore, the decreased expression of the Wnt-beta catenin inhibitor DKK1, which can be induced by p53, was also observed [31]. Whether GLDN regulates tumor cell proliferation through the Wnt pathway remains an unresolved question. To fully understand the role of p53-mediated apoptosis in the context of GLDN's effects, further research is needed to explore if the inhibition of cell growth due to GLDN knockdown involves p53-mediated cell death.

A comprehensive exploration of target genes implicated in tumorigenesis and critical signaling pathways holds the potential to serve as a foundational platform for identifying novel inhibitors. This approach has the potential to catalyze the development of innovative therapeutic strategies with significant practical implications, thereby accelerating advance in clinical application research. We believe that further investigation into GLDN could offer new insights into GC and unveil new targets for prognostic assessement in GC patients.

Data availability statement

The raw data of RNA-seq are available via the NCBI's Sequence Read Archive (SRA) accession number BioProject PRJNA1155917.

Ethics approval and consent to participate

All animal experiments were approved by the Experimental Animal Ethics Committee of Jining Medical University (approval no.

JNMC-2021-DW-067).

CRediT authorship contribution statement

Xue You: Writing – review & editing, Writing – original draft, Validation, Supervision, Software, Resources, Project administration, Methodology, Investigation, Funding acquisition, Data curation, Conceptualization. **Minghe Wang:** Methodology, Investigation, Data curation, Conceptualization. **Xuejing Wang:** Methodology, Investigation, Data curation. **Xiaotong Wang:** Methodology, Investigation, Data curation. **Yuting Cheng:** Investigation, Data curation. **Chuan Zhang:** Methodology, Investigation. **Qingrun Miao:** Methodology, Data curation. **Ying Feng:** Writing – review & editing, Visualization, Validation, Supervision, Software, Project administration, Investigation, Conceptualization.

Declaration of competing interest

The authors declare that they have no known competing financial interests or personal relationships that could have appeared to influence the work reported in this paper.

Acknowledgements

We would like to express my thanks to Editage (www.editage.cn) for English language editing and the Beijing Genomics Institute (www.genomics.org.cn) for RNA-seq. This work was supported by grants from the Shandong Provincial Natural Science Foundation (ZR2021QH151) and the Medicine and Health Care Science and Technology Development Plan Projects Foundation of Shandong Province (202002080986).

Appendix A. Supplementary data

Supplementary data to this article can be found online at https://doi.org/10.1016/j.heliyon.2024.e38153.

References

[1] F. Bray, J. Ferlay, I. Soerjomataram, R.L. Siegel, L.A. Torre, A. Jemal, Global cancer statistics 2018: GLOBOCAN estimates of incidence and mortality worldwide for 36 cancers in 185 countries, CA Cancer J Clin 68 (6) (2018) 394–424.
[2] Y. Zhang, J. Yu, The role of MRI in the diagnosis and treatment of gastric cancer, Diagn Interv Radiol 26 (3) (2020) 176–182.
[3] A.P. Thrift, H.B. El-Serag, Burden of gastric cancer, Clin. Gastroenterol. Hepatol. 18 (3) (2020) 534–542.
[4] C. Mattiuzzi, G. Lippi, Current cancer epidemiology, J Epidemiol Glob Health 9 (4) (2019) 217–222.
[5] J.Y. Hwang, Y.J. Kim, B.Y. Choi, B.J. Kim, B.G. Han, Meta analysis identifies a novel susceptibility locus associated with heel bone strength in the Korean population, Bone 84 (2016) 47–51.
[6] J. Maluenda, C. Manso, L. Quevarec, A. Vivanti, F. Marguet, M. Gonzales, F. Guimiot, F. Petit, A. Toutain, S. Whalen, R. Grigorescu, A.D. Coeslier, M. Gut, I. Gut, A. Laquerriere, J. Devaux, J. Melki, Mutations in GLDN, encoding gliomedin, a critical component of the nodes of ranvier, are responsible for lethal arthrogryposis, Am. J. Hum. Genet. 99 (4) (2016) 928–933.
[7] L. Gao, Z. Guan, P. Gao, W. Zhang, Q. Qi, X. Lu, Cytophaga hutchinsonii gldN, encoding a core component of the type IX secretion system, is essential for ion assimilation, cellulose degradation, and cell motility, Appl. Environ. Microbiol. 86 (11) (2020).
[8] C.R. Graveel, S.R. Harkins-Perry, L.G. Acevedo, P.J. Farnham, Identification and characterization of CRG-L2, a new marker for liver tumor development, Oncogene 22 (11) (2003) 1730–1736.
[9] Q. Zhang, J. Wang, M. Liu, Q. Zhu, Q. Li, C. Xie, C. Han, Y. Wang, M. Gao, J. Liu, Weighted correlation gene network analysis reveals a new stemness index-related survival model for prognostic prediction in hepatocellular carcinoma, Aging (Albany NY) 12 (13) (2020) 13502–13517.
[10] L. Chen, D. Lu, K. Sun, Y. Xu, P. Hu, X. Li, F. Xu, Identification of biomarkers associated with diagnosis and prognosis of colorectal cancer patients based on integrated bioinformatics analysis, Gene 692 (2019) 119–125.
[11] H. Chen, M. Yang, Q. Wang, F. Song, X. Li, K. Chen, The new identified biomarkers determine sensitivity to immune check-point blockade therapies in melanoma, OncoImmunology 8 (8) (2019) 1608132.
[12] W. Chen, W. Li, Z. Liu, G. Ma, Y. Deng, L. Zhu, Q. Zhou, Identification of tumor microenvironment-based genes associated with acquired resistance to EGFR Tyrosine Kinase Inhibitor in Lung Adenocarcinoma, J. Cancer 13 (3) (2022) 877–889.
[13] B. Ru, C.N. Wong, Y. Tong, J.Y. Zhong, S.S.W. Zhong, W.C. Wu, K.C. Chu, C.Y. Wong, C.Y. Lau, I. Chen, N.W. Chan, J. Zhang, TISIDB: an integrated repository portal for tumor-immune system interactions, Bioinformatics 35 (20) (2019) 4200–4202.
[14] L. Yao, J. Li, Z. Xu, Y. Yan, K. Hu, GSDMs are potential therapeutic targets and prognostic biomarkers in clear cell renal cell carcinoma, Aging (Albany NY) 14 (6) (2022) 2758–2774.
[15] B. Gyorffy, Survival analysis across the entire transcriptome identifies biomarkers with the highest prognostic power in breast cancer, Comput. Struct. Biotechnol. J. 19 (2021) 4101–4109.
[16] Z. Ma, D. Liu, W. Li, S. Di, Z. Zhang, J. Zhang, L. Xu, K. Guo, Y. Zhu, J. Han, X. Li, X. Yan, STYK1 promotes tumor growth and metastasis by reducing SPINT2/HAI-2 expression in non-small cell lung cancer, Cell Death Dis. 10 (6) (2019) 435.
[17] K. Meng, J. Cao, Y. Dong, M. Zhang, C. Ji, X. Wang, Application of bioinformatics analysis to identify important pathways and hub genes in ovarian cancer affected by WT1, Front. Bioeng. Biotechnol. 9 (2021) 741051.
[18] J. Ye, J. Zha, Y. Shi, Y. Li, D. Yuan, Q. Chen, F. Lin, Z. Fang, Y. Yu, Y. Dai, B. Xu, Co-inhibition of HDAC and MLL-menin interaction targets MLL-rearranged acute myeloid leukemia cells via disruption of DNA damage checkpoint and DNA repair, Clin Epigenetics 11 (1) (2019) 137.
[19] V. Tandon, L. de la Vega, S. Banerjee, Emerging roles of DYRK2 in cancer, J. Biol. Chem. 296 (2021) 100233.
[20] R. Keough, E. Woollatt, J. Crawford, G.R. Sutherland, S. Plummer, G. Casey, T.J. Gonda, Molecular cloning and chromosomal mapping of the human homologue of MYB binding protein (P160) 1A (MYBBP1A) to 17p13.3, Genomics 62 (3) (1999) 483–489.
[21] H. Ali, J.M. Zmuda, R.K. Cvejkus, E.E. Kershaw, A.L. Kuipers, E.A. Oczypok, V. Wheeler, C.H. Bunker, I. Miljkovic, Wnt pathway inhibitor DKK1: a potential novel biomarker for adiposity, J Endocr Soc 3 (2) (2019) 488–495.

[22] J. Bockhorn, A. Prat, Y.F. Chang, X. Liu, S. Huang, M. Shang, C. Nwachukwu, M.J. Gomez-Vega, J.C. Harrell, O.I. Olopade, C.M. Perou, H. Liu, Differentiation and loss of malignant character of spontaneous pulmonary metastases in patient-derived breast cancer models, Cancer Res. 74 (24) (2014) 7406–7417.
[23] T. Daubon, C. Leon, K. Clarke, L. Andrique, L. Salabert, E. Darbo, R. Pineau, S. Guerit, M. Maitre, S. Dedieu, A. Jeanne, S. Bailly, J.J. Feige, H. Miletic, M. Rossi, L. Bello, F. Falciani, R. Bjerkvig, A. Bikfalvi, Deciphering the complex role of thrombospondin-1 in glioblastoma development, Nat. Commun. 10 (1) (2019) 1146.
[24] L. Chen, J. Li, Y. Fan, J. Qiu, L. Cao, R. Laurent, S. Mignani, A.M. Caminade, J.P. Majoral, X. Shi, Revisiting cationic phosphorus dendrimers as a nonviral vector for optimized gene delivery toward cancer therapy applications, Biomacromolecules 21 (6) (2020) 2502–2511.
[25] T. Takeuchi, M. Hattori-Kato, Y. Okuno, M. Zaitsu, T. Azuma, Genome-wide association study adjusted for occupational and environmental factors for bladder cancer susceptibility, Genes 13 (3) (2022).
[26] A.J. Levine, W. Hu, Z. Feng, The P53 pathway: what questions remain to be explored? Cell Death Differ. 13 (6) (2006) 1027–1036.
[27] S.L. Harris, A.J. Levine, The p53 pathway: positive and negative feedback loops, Oncogene 24 (17) (2005) 2899–2908.
[28] H. Hirata, et al., Wnt antagonist DKK1 acts as a tumor suppressor gene that induces apoptosis and inhibits proliferation in human renal cell carcinoma, Int. J. Cancer 128 (8) (2011) 1793–1803.
[29] J. Liu, C.Y. Qin, VX-680 induces p53-mediated apoptosis in human cholangiocarcinoma cells, Anti Cancer Drugs 29 (10) (2018) 1004–1010.
[30] M.E. Bowen, A.S. Mulligan, A. Sorayya, L.D. Attardi, Puma- and Caspase9-mediated apoptosis is dispensable for p53-driven neural crest-based developmental defects, Cell Death Differ. 28 (7) (2021) 2083–2094.
[31] J. Wang, J. Shou, X. Chen, Dickkopf-1, an inhibitor of the Wnt signaling pathway, is induced by p53, Oncogene 19 (14) (2000) 1843–1848.